Influence of Thermoplastic Elastomers on Mechanical Properties and Morphologies of Isotactic Polypropene/Glass Bead Hybrid Composites

F. STRICKER and R. MÜLHAUPT*

Freiburger Materialforschungszentrum und Institut für Makromolekulare Chemie der Albert-Ludwigs-Universität, Stefan-Meier-Straße 21, D-79104 Freiburg i. Br., Germany

SYNOPSIS

Glass bead-reinforced isotactic polypropene hybrid composites containing 0–20 vol % thermoplastic elastomers were prepared to study both structure/property relationships and morphology development. Polystyrene-*block*-poly(ethene-*co*-but-1-ene)-*block*-polystyrene (SEBS) and the corresponding block copolymer grafted with maleic anhydride (SEBS-*g*-MA) were used as thermoplastic elastomers. Hybrid composites containing SEBS gave higher Young's moduli than did those containing SEBS-*g*-MA. The experimental Young's moduli were in good agreement with the theoretical predictions according to Lewis and Nielsen. The lower moduli of hybrid composites containing SEBS-*g*-MA were attributed to interlayer formation and *in situ* encapsulation of glass beads, resulting in core–shell particles. This elastomeric interlayer impaired the filler reinforcement. Analysis of tensile yield stress and results of lap-shear tests confirmed strong filler–polymer interactions in composites containing SEBS-*g*-MA. Only in excess of a critical volume fraction did SEBS-*g*-MA afford a significant improvement of the notched Izod impact strength. In contrast to stiffness, Izod impact strength was not influenced by the type of elastomer and morphology. Investigations of crystallization and scanning electron microscopic studies proved the *in situ* encapsulation of the glass beads with SEBS-*g*-MA, whereas SEBS addition results in separately dispersed glass beads and SEBS microphases. © 1996 John Wiley & Sons, Inc.

INTRODUCTION

Isotactic polypropene (i-PP) is used in a wide range of applications because of its attractive combination of low price, heat distortion temperature above 100°C, and high stiffness. However, poor impact strength of PP, especially at low temperatures, limits its use in some applications. Therefore, it is common practice to toughen PP by incorporating elastomer microparticles, e.g., by physical blending of PP with elastomers.[1,2] Since soft elastomeric phases reduce the modulus of PP blends, reinforcing fillers are added to improve the balance of impact strength and stiffness of the resulting hybrid composites. Talcum and calcium carbonate are widely applied as reinforcing components.[3–7] Because of their anisotropy and very regular shape, glass beads are used for model systems and theoretical investigations.[8,9] In 1969, Matonis and Small[10] proposed that the encapsulation of rigid spherical inclusions within a thin layer of a low modulus elastomer could afford hybrid composites exhibiting improved toughness without sacrificing stiffness with respect to the PP matrix.

The present article describes the influence of thermoplastic elastomers on the morphology development and mechanical properties, e.g., stiffness, strength, and toughness, as well as the crystallization behavior of glass bead-reinforced PP. Two thermoplastic elastomers (TPE) were used: polystyrene-*block*-poly(ethene-*co*-but-1-ene)-*block*-polystyrene (SEBS) and the corresponding block copolymer grafted with maleic anhydride (SEBS-*g*-MA). Aminopropyl-functionalized glass beads of 5 μm average

* To whom correspondence should be addressed.

Journal of Applied Polymer Science, Vol. 62, 1799–1806 (1996)
© 1996 John Wiley & Sons, Inc. CCC 0021-8995/96/111799-08

Table I Mechanical Properties of PP Hybrid Composites with Glass Beads and Thermoplastic Elastomer

Glass Spheres (Vol %)	SEBS (Vol %)	SEBS-*g*-MA (Vol %)	Young's Modulus (MPa)	Yield Stress (MPa)	Elongation to Break (%)	Notched Izod Impact Strength (kJ/sqm)
—	—	—	1108	33.0	640	4.2
10	—	—	1269	27.7	180	3.7
10	2.5	—	1249	26.1	420	5.8
10	5	—	1188	25.0	370	6.3
10	10	—	1122	22.7	350	8.9
10	20	—	921	18.2	390	24.1
10	—	2.5	1188	29.5	370	5.3
10	—	5	1071	27.4	360	7.9
10	—	10	904	24.3	340	8.4
10	—	20	730	18.6	400	17.5

diameter were blended together with isotactic PP in a twin-screw kneader with counterrotating screws at 60 rpm and 240°C. The morphology and mechanical properties were studied as a function of both type and volume fraction of the TPE.

EXPERIMENTAL

Materials

All polymers were commercial grades, supplied by Shell, and used without further purification: isotactic polypropene (i-PP; KM 6100, M_n = 46,500 g/mol; M_w/M_n = 7.6, MFI = 3.5 g/10 min at 230°C), polystyrene-*block*-poly(ethene-*co*-but-1-ene)-*block*-polystyrene (Kraton G1652, abbreviated SEBS, M_n = 90,000 g/mol, polystyrene content of 29 wt %), and the corresponding maleinated SEBS-*g*-MA (Kraton FG1901X, grafted with 2 wt % maleic anhydride). Aminopropyl-functional glass beads (Potters-Ballotini 5000 CP-03, average diameter of 5 μm), containing 0.02 wt % coating of aminopropyltrimethoxysilane were used as the filler component; 0.2 wt % Irganox 1010/Irgafos 168 (4/1 wt %) were added as stabilizers during the melt processing.

Preparation of Hybrid Composites

All composites were prepared under identical mixing and molding conditions. TPE volume fractions were varied between 0 and 20 vol %. The filler content was maintained at 10 vol %. Melt blending was performed in a Haake Rheomix 90 twin-screw kneader equipped with a 60 mL mixing chamber that was preheated at 240°C. Typically, PP was molten together with the stabilizers for 1.5 min. Then, the filler was added, followed 1 min later by TPE. After 4 min total mixing time, the sample was quickly recovered and quenched between metal plates. Sheets of 2 mm thickness were prepared by compression molding in an evacuated press (Schwabenthan Polystat 100), annealing at 250°C for 10 min and quenching to ambient temperature between water-cooled metal plates. Rectangular bars of a dimension of 60 × 10 × 2 mm were cut out of these plates for the evaluation of mechanical properties.

Mechanical Tests

Tensile properties were measured on an Instron (Model 4202) tensile machine according to the DIN 53455 standard procedure using a test specimen of 2 mm thickness and a crosshead speed of 10 mm/min. Notched Izod impact strength values were determined on notched samples according to ISO 180/1A using a test specimen of 60 × 10 × 2 mm. The average standard deviations of the Young's modulus and yield stress were approximately 5%; of impact strength, 10%; and of elongation to break, 30%. At least five samples were tested for each composite composition, and the average value is reported. Tests were performed at ambient temperature (23 ± 2°C).

Lap Shear Test

Thin Kraton films of approximate 0.1 mm thickness were pressed at 200°C under vacuum and cooled down rapidly to room temperature. Two glass plates of 80 × 10 mm were washed three times with chloroform and dried under vacuum at 100°C. About 150 mm^2 of the Kraton film was placed between the ends of the glass plates and pressed for 10 min at

200°C. The specimen was then mounted in the Instron machine. The force necessary to separate the two glass plates is determined at a crosshead speed of 1 mm/min. At least five specimens were measured and the average force normalized by the area of the interface to calculate the lap shear strength (MPa).

Thermal Analysis

Thermal properties such as melting temperature, melting enthalpy, crystallization temperature, and crystallization enthalpy were recorded on a Perkin–Elmer DSC-7 using a heating rate of 10 K/min. Prior to measurement, the samples were heated 5 min at 200°C and then cooled to 135°C using a heating rate of 3 K/min. The annealing time at 135°C was 12 h to achieve isothermal crystallization conditions. To investigate nucleation behavior in more detail, small amounts of the samples were molten and pressed between two glass slides to form a thin film of approximately 30 μm thickness. After annealing at 200°C for 3 min using a hot stage (Lickham THM600), the samples were cooled at 30 K/min to reach 135°C for isothermal crystallization. The crystallization was observed using a polarized light in an Olympus AH-2 optical microscope, measuring the relative intensity by means of a photocell. The measurement was completed when the light intensity remained constant for 5 min.

Scanning Electron Microscopy (SEM)

The morphology of the hybrid composites was determined using SEM. The fracture surfaces of impact tests sputtered with gold were investigated using an electron microscope DSM 960 of Zeiss. The acceleration voltage was 20 kV.

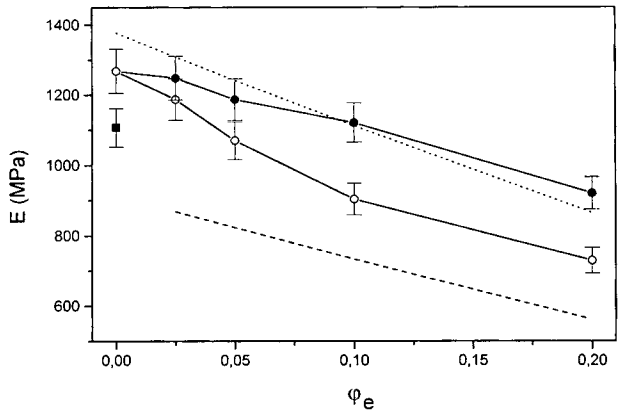

Figure 1 Comparison of experimental data with theoretical predictions for the composite composition dependence of the Young's modulus E: (■) PP; (●) PP with 10 vol % glass beads and SEBS; (○) PP with 10 vol % glass beads and SEBS-g-MA; (· · ·) theoretical data according to Lewis–Nielsen equation [eq. (1)]; (– – –) theoretical data according to equation for lower boundary [eq. (9)].

RESULTS AND DISCUSSION

Tensile Properties

The Young's modulus, measured as slope of the stress–strain curve, tensile strength, and notched Izod impact strength were determined as a function of TPE type and volume fraction. The results are listed in Table I and illustrated in Figures 1, 3 and 5.

The dependence of the Young's modulus on the TPE volume fraction (φ_e) is depicted in Figure 1. As expected, the hybrid composite moduli decrease with increasing TPE volume fraction. The stiffness of the hybrid composites containing SEBS is always higher than that of the corresponding hybrid composites containing SEBS-g-MA, especially at high TPE volume fraction.

Modulus data were compared with theoretical predictions for three-phase hybrid composites, containing separately dispersed TPE and the filler in the PP matrix. The influence of the filler and TPE volume fractions on the Young's modulus are calculated independently and combined in one equation. The dotted line in Figure 1 was calculated by the extended Lewis–Nielsen equation[11–13] [eq. (1)]:

$$E = E_m \times \frac{1 - \Psi_e B_e \varphi'_e}{1 + A_e B_e \varphi_e} \times \frac{1 + A_f B_f \varphi_f}{1 - \Psi_f B_f \varphi_f} \qquad (1)$$

where E and E_m are composite and polypropene moduli. φ'_e is given as

$$\varphi'_e = \frac{\varphi_e}{1 - \varphi_f} \qquad (2)$$

where φ_e and φ_f are the volume fractions of thermoplastic elastomer and filler, respectively (appendix m, e, and f corresponding to matrix, elastomer, and filler). According to the theory, A_e, A_f, B_e, and B_f are expressed by eqs. (3), (4), (5), and (6):

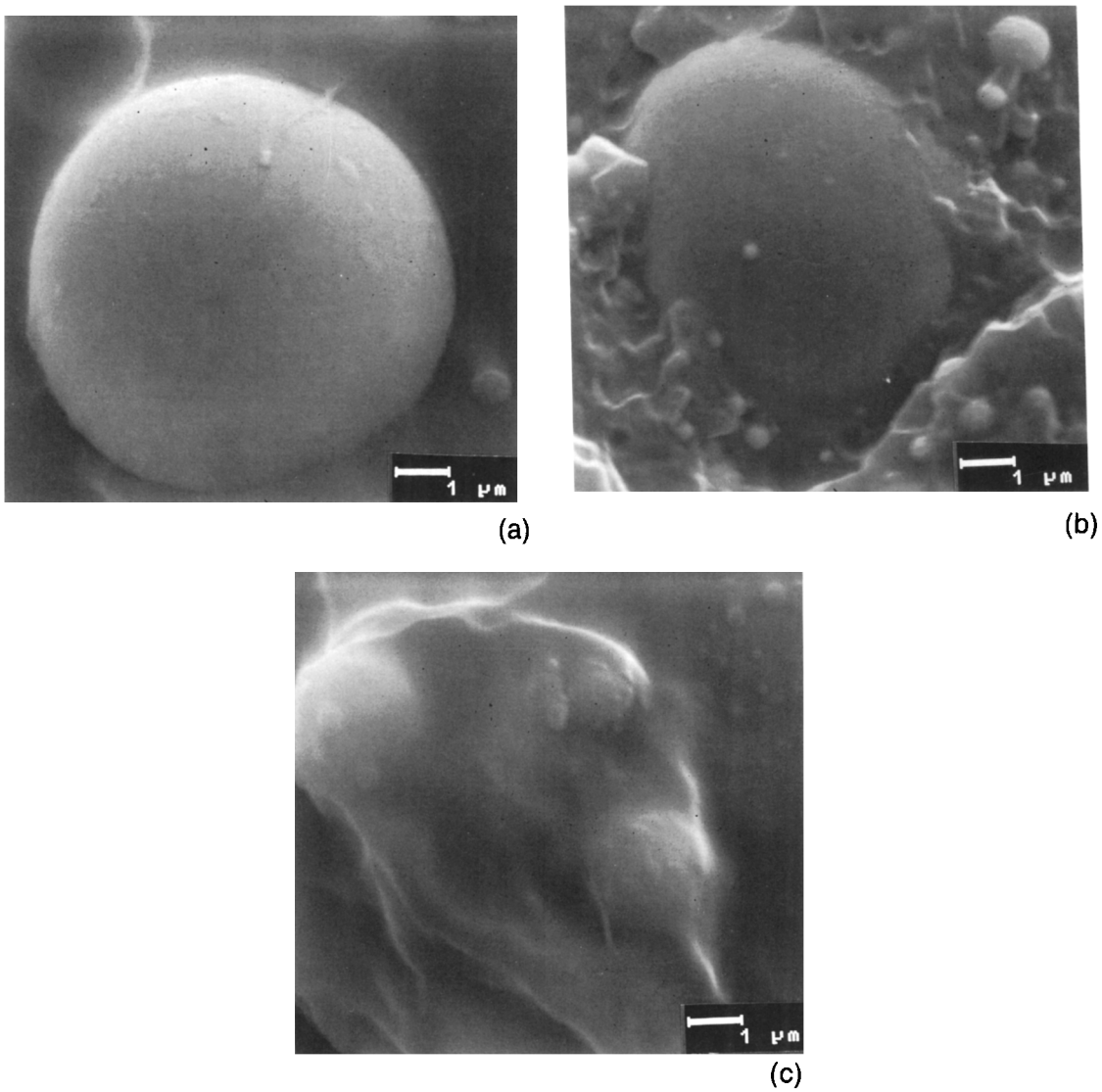

Figure 2 Scanning electron micrographs of fractured surfaces of PP hybrid composites containing (a) 10 vol % glass beads and 2.5 vol % SEBS; (b) 10 vol % glass beads and 2.5 vol % SEBS-*g*-MA, and (c) 10 vol % glass beads and 10 vol % SEBS-*g*-MA.

$$A_e = \frac{8 - 10\nu_m}{7 - 5\nu_m} \tag{3}$$

$$A_f = \frac{7 - 5\nu_m}{8 - 10\nu_m} \tag{4}$$

$$B_e = \frac{E_m - E_e}{E_m + A_e E_e} \tag{5}$$

$$B_f = \frac{E_f - E_m}{E_f + A_f E_m} \tag{6}$$

In the equations, E_e and E_f are the moduli of the dispersed TPE and the filler and ν_m is the Poisson ratio of the PP matrix. The parameters Ψ_e and Ψ_f take into account the maximum packing fraction of the elastomer, Ψ_e^{max}, and filler, Ψ_f^{max}, in the case of spherical particles[12]:

$$\Psi_e = 1 + \left[\frac{1 - \varphi_e^{max}}{\varphi_e^{max2}}\right]\varphi_e' \tag{7}$$

$$\Psi_f = 1 + \left[\frac{1 - \varphi_f^{max}}{\varphi_f^{max2}}\right]\varphi_f \tag{8}$$

The parameters of the materials used in this study are listed in Table II.

In the case of core–shell morphologies, the effective TPE volume fraction increases while the stiff-

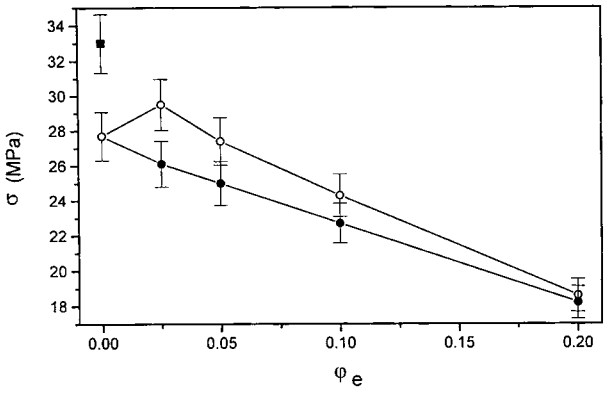

Figure 3 Yield stress σ as a function of TPE volume fraction φ_e of PP hybrid composites: (■) PP; (●) PP with 10 vol % glass beads and SEBS; (○) PP with 10 vol % glass beads and SEBS-*g*-MA.

ening effect of the filler is reduced with increasing thickness of the elastomer shell. The different morphologies are illustrated in Figure 4.

The Lewis–Nielsen equation for the resulting two-phase hybrid composites with core–shell particles can be modified [eq. (9)] and represents, thus, the lower boundary:

$$E = E_m \times \frac{1 - \Psi_e B_e(\varphi_e + \varphi_f)}{1 + A_e B_e(\varphi_e + \varphi_f)} \qquad (9)$$

The data for hybrid composites with SEBS containing separately dispersed filler and SEBS phases fit the extended Lewis–Nielsen equation for a three-phase morphology. The data of hybrid composites with SEBS-*g*-MA are between the extended Lewis–Nielsen equation and the equation of the lower boundary corresponding to the two-phase morphology. From these results, we conclude that SEBS is dispersed as a separate phase, whereas SEBS-*g*-MA encapsulates glass beads to form core–shell particles consisting of a glass bead core and a TPE shell. Interlayer formation could result from interfacial adhesion, e.g., *in situ* coupling of succinic–anhydride groups.

Table II Parameters of the Materials Used in This Study

	E (MPa)	ν	$\Psi_{max.}$
i-PP	1108	0.35[12]	—
SEBS	20	—	0.64
SEBS-*g*-MA	20	—	0.64
Glass beads	68,950[a]	—	0.64

[a] Information from the manufacturer of the glass beads: Potter-Ballotini.

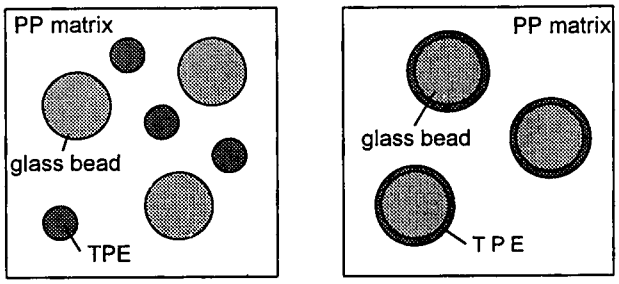

Figure 4 Morphologies of PP hybrid composites: (a) three-phase morphology with separately dispersed elastomer and filler particles; (b) two-phase morphology with core–shell particles (filler particle core and an elastomeric shell).

Scanning electron microscopic studies of fracture surfaces of PP hybrid composites containing glass beads and TPE are presented in Figure 2(a)–(c). Hybrid composites containing 10 vol % glass beads and 2.5 vol % SEBS show poor adhesion between filler and PP matrix [Fig. 2(a)]. This is in accordance with the poor adhesion of SEBS on glass. In contrast, SEBS-*g*-MA displays much better interfacial adhesion. SEM images of fracture surfaces of hybrid composites, containing 10 vol % glass beads and 2.5 vol % SEBS-*g*-MA, clearly indicate that cracks propagate through the PP matrix [Fig. 2(b)]. The surface of the filler particles is very diffuse, due to formation of the TPE shell. In fact, at 10 vol % SEBS-*g*-MA, glass beads cannot be detected at the fracture surface [Fig. 2(c)].

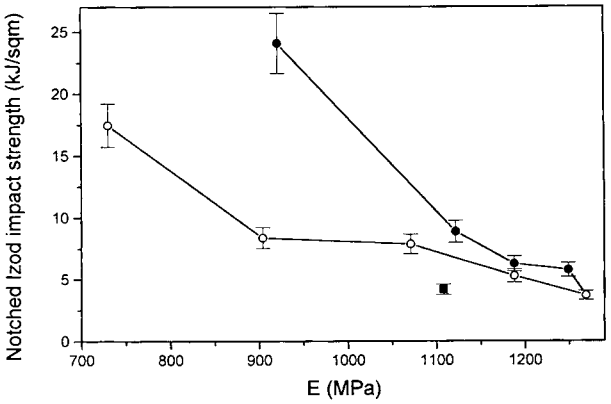

Figure 5 Young's modulus *E* correlated with notched Izod impact strength of PP hybrid composites containing different volume fractions of TPE which varies from left to the right from 20 to 10, 5, 2.5, 0 vol % and the following filler volume fractions and the TPE types: (■) PP without modifiers; (●) 10 vol % glass beads and SEBS; (○) 10 vol % glass beads and SEBS-*g*-MA.

Table III Thermal Properties of PP Hybrid Composites with Glass Beads and Kraton Estimated from DSC Studies

Glass Spheres (Vol %)	SEBS (Vol %)	SEBS-*g*-MA (Vol %)	T_{cryst} (°C)	ΔH_{cryst} (J/g)	T_m (°C)	ΔH_m (J/g)
—	—	—	110.6	−93.4	169.7	108.0
10	—	—	117.1	−93.4	171.6	108.3
10	2.5	—	117.0	−93.2	171.2	111.9
10	5	—	116.7	−92.8	170.4	110.5
10	10	—	116.7	−91.0	171.6	107.2
10	20	—	116.5	−90.6	171.0	105.5
10	—	2.5	114.6	−92.2	169.8	106.9
10	—	5	113.8	−89.9	170.6	105.5
10	—	10	114.2	−88.6	170.5	103.2
10	—	20	114.0	−88.5	171.1	99.8

Yield stress and tensile strength, measured at large deformations, are more extensively dependent upon interfacial adhesion with respect to the Young's modulus, measured at very small deformations. For instance, tensile yield stress proved to be an excellent property to correlate with interfacial interactions in heterogeneous polymer systems.[14] Pukanszky[15] calculated a parameter related to stress transfer of filled polymers. The morphology of three-phase hybrid composites is too complex and makes determination of such parameters difficult. Nevertheless, analysis of yield stress offers information about interfacial interactions. In Figure 3, yield stress is plotted against the TPE volume fraction. The yield stress of PP hybrid composites containing SEBS decreases with increasing TPE volume fraction.

At small volume fractions of SEBS-*g*-MA of 5 vol %, a distinct yield stress increase was observed before encountering decays at higher SEBS-*g*-MA volume fractions. In comparison to SEBS, SEBS-*g*-MA gave, as expected, much higher yield stresses and improved interfacial adhesion due to the *in situ* filler encapsulation. Influence of SEBS-*g*-MA, on both the Young's modulus and yield stress, indicate that SEBS-*g*-MA accumulates at the filler surface and forms an elastomeric interlayer. Only small volume fractions, about 2.5 vol %, of SEBS-*g*-MA are necessary to form this interlayer and to promote efficient coupling between the filler and PP matrix. A lap shear test was used to investigate macroscopic interactions between glass and TPE in more detail. The lap shear strength, necessary to separate glass and the thin SEBS film, is 0.9 MPa. In comparison, the corresponding lap shear strength of SEBS-*g*-MA

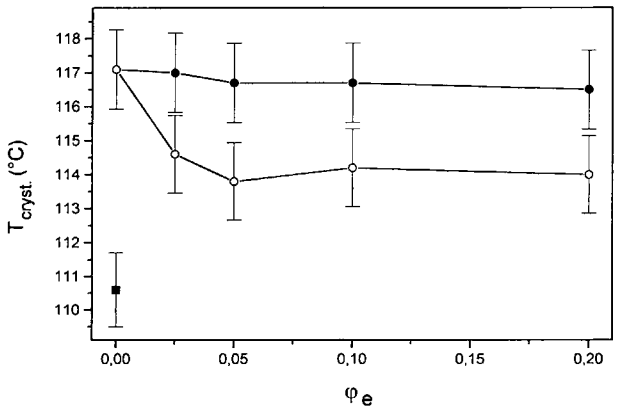

Figure 6 Crystallization temperature $T_{cryst.}$ as a function of thermoplastic elastomer volume fraction φ_e: (■) PP; (●) PP with 10 vol % glass beads and SEBS; (○) PP with 10 vol % glass beads and SEBS-*g*-MA.

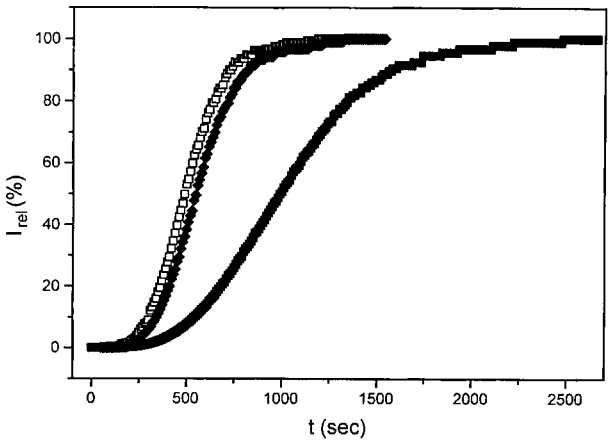

Figure 7 Isothermal crystallization of PP composites with glass beads at 135°C, monitored via variation of polarized light intensity I_{rel} as a function of time t: (■) PP without modifiers; (♦) PP containing 10 vol % glass beads; (□) PP containing 20 vol % glass beads.

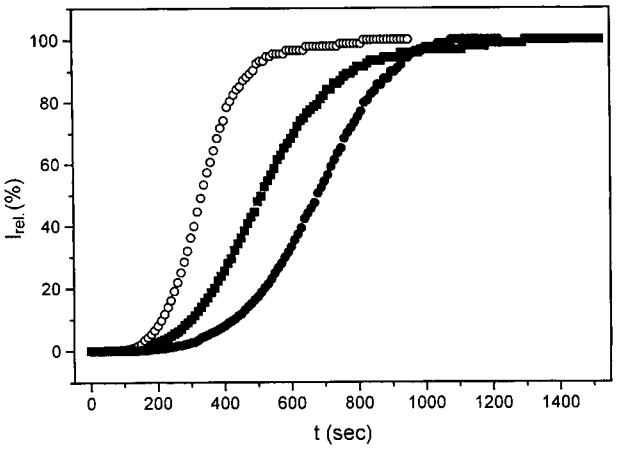

Figure 8 Isothermal crystallization of PP hybrid composites with glass beads at 135°C, monitored via variation of polarized light intensity I_{rel} as a function of time t: (■) PP containing 10 vol % glass beads; (○) PP containing 10 vol % glass beads and 10 vol % SEBS; (●) PP containing 10 vol % glass beads and 10 vol % SEBS-*g*-MA.

on glass is 2.3 MPa, more than twice as much when compared to that of SEBS. This is due to the polar interactions of succinic anhydride with the filler surface. Moreover, the amino-functional filler surface of the glass beads can form covalent bonds with SEBS-*g*-MA via imide groups, resulting in stronger interactions in the hybrid composites.

Impact Properties

Impact strength of PP hybrid composites with glass beads slightly increases with the TPE volume fraction. To achieve significant improvement in the impact strength, large amounts of about 20 vol % of SEBS or SEBS-*g*-MA are required. In accordance with results of Dekkers et al.,[16] who investigated PP/glass bead composites containing polystyrene-*block*-polybutadiene-*block*-polystyrene, rubbery interlayers do not appear to improve toughness. In Figure 5, notched Izod impact strength is plotted against the Young's modulus. SEBS-*g*-MA gave a poor toughness/stiffness balance compared to that of SEBS. Clearly, elastomeric interlayers adversely affect matrix reinforcement without, simultaneously, improving resistance to crack propagation.

Crystallization Behavior

The investigations of morphological and mechanical properties provide strong experimental evidence for the existence of SEBS-*g*-MA interlayers which should also affect PP nucleation. The melting and crystallization behaviors of PP hybrid composites were investigated as a function of the SEBS and SEBS-*g*-MA volume fractions. The results are listed in Table III. Glass beads are nucleating PP as demonstrated by differential scanning calorimetric studies. The nucleating effect is reflected by higher crystallization temperatures when cooling molten PP hybrid composites. Addition of SEBS affected marginally the nucleation, while SEBS-*g*-MA distinctly lowers crystallization temperatures of PP. As shown in Figure 6, small SEBS-*g*-MA volume fractions were sufficient to reduce nucleation of glass bead-based PP hybrid composites, whereas a higher volume fraction did not further affect nucleation. This is again experimental evidence for elastomeric interlayer formation in the case of compatibilized SEBS-*g*-MA.

This influence on nucleation was further studied by polarized light microscopy on PP composites crystallized isothermally at 135°C. In Figures 7 and 8, the crystallization rate, expressed by the relative light intensity as a function of time, is monitored for PP hybrid composites. As shown in Figure 7, glass beads have a distinct nucleation effect on PP. In Figure 8, 10 vol % SEBS or SEBS-*g*-MA were added. Clearly, SEBS-*g*-MA slows down PP crystallization by reducing nucleation capacity via *in situ* filler encapsulation. In contrast, SEBS accelerates nucleation, as the separate SEBS microparticles function also as nucleating agents.

CONCLUSION

The influence of the TPE type and its volume fraction on mechanical and thermal properties as well as on the fracture surface aspect indicate that different morphologies are obtained for PP/glass bead hybrid composites blended with SEBS or SEBS-*g*-MA. Hybrid composites containing SEBS gave much higher Young's moduli with respect to those containing SEBS-*g*-MA. This is attributed to formation of SEBS-*g*-MA interlayers between the filler and PP matrix. The modulus of hybrid composites containing separately dispersed SEBS were in good agreement with the predictions of Nielsen and Lewis for three-phase morphology. The modulus of hybrid composites based upon SEBS-*g*-MA was fitted by an equation taking into account core–shell particles equivalent to pure TPE. Analysis of tensile yield stress and lap shear tests indicated good filler–polymer adhesion in composites containing SEBS-*g*-MA. The influence of SEBS on tensile yield stress corresponds to the behavior of the corresponding

PP/SEBS blends. Notched Izod impact strength was almost independent of the type of thermoplastic elastomer and increased strongly at a TPE volume fraction exceeding 10 vol %. Using differential scanning calorimetry and polarized light microscopy, it was possible to demonstrate that SEBS-*g*-MA reduces the nucleating activity of the glass beads. This again reflects formation of TPE interlayers and core–shell morphology. Comparison of SEBS vs. SEBS-*g*-MA clearly indicates that the core–shell morphology obtained with SEBS-*g*-MA is not efficient in increasing the toughness/stiffness balance. Three-phase morphology, containing separately dispersed filler and TPE, give hybrid composites exhibiting an improved combination of stiffness and toughness.

The authors would like to thank Shell Research in Louvain-la-Neuve, Belgium—in particular, A. Farina—for supporting this study.

REFERENCES

1. B. Pukanszky and F. Tüdös, *Makromol. Chem. Macromol. Symp.*, **38,** 221–231 (1990).
2. F. C. Stehling, T. Huff, C. Speed, and G. Wissler, *J. Appl. Polym. Sci.*, **26,** 2693–2711 (1981).
3. F. Stricker and R. Mülhaupt, *High Perform. Polym.*, **8,** 97–108 (1996).
4. S. N. Maiti and P. K. Mahapatro, *J. Appl. Polym. Sci.*, **42,** 3101–3110 (1991).
5. J. E. Stamhuis, *Polym. Comp.*, **5,** 202 (1984).
6. J. E. Stamhuis, *Polym. Comp.*, **9,** 72–77 (1988).
7. S. N. Maiti and K. K. Sharma, *J. Mater. Sci.*, **27,** 4605–4613 (1992).
8. J. Rösch, P. Barghoorn, and R. Mülhaupt, *Rapid Commun.*, **15**(9), 691–696 (1994).
9. F. Ramsteiner and R. Theysohn, *Composites,* **15,** 121–128 (1984).
10. V. A. Matonis and N. C. Small, *Polym. Eng. Sci.*, **9,** 90–98 (1969).
11. E. H. Kerner, *Proc. Phys. Soc.*, **69,** 808–813 (1956).
12. W.-Y. Chiang, W. D. Yang, and B. Pukanszky, *Polym. Eng. Sci.*, **32,** 641 (1992).
13. J. Kolarik and J. Jancar, *Polymer,* **33,** 4961–4967 (1992).
14. T. S. Chow, *J. Polym. Sci. Polym. Phys. Ed.*, **20,** 2103–2109 (1982).
15. B. Pukanszky, *Composites,* **21,** 255–262 (1990).
16. M. E. J. Dekkers, J. P. M. Dortmans, and D. Heikens, *Polym. Commun.*, **26,** 145–148 (1985).

Received February 5, 1996
Accepted May 20, 1996